JOURNAL OF GEOPHYSICAL RESEARCH, VOL. 102, NO. D7, PAGES 8887–8898, APRIL 20, 1997

The atmospheric column abundance of IO: Implications for stratospheric ozone

P. O. Wennberg,[1] J. W. Brault,[2,3] T. F. Hanisco,[1] R. J. Salawitch,[4] and George H. Mount[2]

Abstract. Absorption attributable to atmospheric IO is observed in high-resolution, high air mass solar spectra taken at the National Solar Observatory, Kitt Peak, Arizona, in March 1995. These observations, together with cross sections measured in the laboratory for the IO {$A\,^2\Pi_{3/2} \leftarrow X\,^2\Pi_{3/2}$ (2,0)} rotationally resolved electronic transition, are consistent with a total stratospheric iodine mixing ratio of 0.2 (+0.3 –0.2) parts per trillion by volume. This result, combined with recent laboratory measurements of the rate of the reactions of IO with other halogen species, suggests that iodine chemistry is not responsible for the reductions observed in lower stratospheric ozone during the last several decades.

1. Introduction

During the past several decades, global ozone reductions have been measured by ground- and satellite-based instruments [World Meteorological Organization/United Nations Environment Programme (WMO/UNEP), 1995]. Halogen chemistry is thought to be partially responsible, given the rising burden of stratospheric chlorine. However, neither the absolute magnitude nor the spatial and seasonal variation of the trend in ozone is well understood. In particular, models cannot account for the large losses of ozone (0.6% yr^{-1}) observed in the lower stratosphere [*Solomon et al.*, 1994b]. Recently, *Solomon et al.* [1994a, b] suggested that iodine chemistry may be responsible. If significant concentrations of iodine monoxide (IO) exist in the stratosphere, the reactions of IO with ClO, BrO, and HO_2 would be important catalytic pathways for the destruction of lower stratospheric ozone.

In this study, high-resolution visible wavelength absorption spectroscopy of the atmosphere, using the Sun as a source, is employed to measure the column abundance of stratospheric IO. Although the infrared analog of this technique has been used for many years to study atmospheric trace species [e.g., *Murcray et al.*, 1968; *Rinsland et al.*, 1985], high resolution spectroscopy has not enjoyed much popularity for use in the visible and ultraviolet spectral region, where much lower resolution techniques are typically employed [e.g., *Noxon et al.*, 1979]. For molecules that exhibit narrow spectral absorption features, however, significant advantages in sensitivity and selectivity can be obtained with high-resolution observations. Here we focus on the $A\,^2\Pi_{3/2} \leftarrow X\,^2\Pi_{3/2}$ (2,0) vibrational band of IO near 445 nm. This transition exhibits spectrally narrow absorption features ($\Delta\nu$ = 0.05 cm^{-1}) providing an unambiguous fingerprint from many individual lines of IO. The rotationally resolved absorption cross sections of this band are sufficiently large that if one part per trillion by volume (pptv) of IO existed in the stratosphere, numerous absorption features greater than 1% would be present in the solar spectrum at high solar zenith angles (SZA). We have attempted to observe these features in spectra taken with the high-resolution Fourier transform spectrometer (FTS) at the National Solar Observatory, Kitt Peak, Arizona [*Brault*, 1978]

2. IO A ←X Vibrational Band Cross Sections

IO was first observed spectroscopically in emission by *Vaidya* [1938] from a methyl iodide flame source. *Durie et al.* [1960] used a high-resolution grating spectrograph to assign six vibrational bands of the $A \leftarrow X$ transition of IO. They noted that the rotational features within the 2–0 vibrational band (445 nm), unlike the other bands, were not broadened beyond the resolution of the spectrograph. Subsequently, this transition has been observed with laser-induced fluorescence [*Inoue et al.*, 1983; *Turnipseed et al.*, 1995a] and Doppler-free laser spectroscopy [*Bekooy et al.*, 1983]. In the latter study the natural lifetime of the excited state was observed to scale with rotational energy. For the first 20 rotational levels the natural widths (full width at half maximum, FWHM) are less than 0.04 cm^{-1}. This makes the 2–0 vibrational band a good candidate for high-resolution absorption measurement of the atmospheric column of IO. In this work, solar spectra were obtained at a resolution of 0.053 cm^{-1}. Determination of the effective cross section for IO at this resolution requires knowledge of the spectral lineshapes that will be a convolution of the instrument resolution and broadening due to Doppler, lifetime, and collisional processes.

Relatively few measurements of the integrated vibrational band cross section of the $A \leftarrow X$ (2–0) transition are available. There are, however, numerous laboratory measurements of the absolute absorption cross sections for the strongest vibrational band (4–0) that, combined with the calculated Franck-Condon factors, provide a means of determining the applicable band cross section. Measured cross sections for the (4–0) band are in good agreement [*Cox and Coker*, 1983; *Jenkin and Cox*, 1985; *Sander*, 1986; *Stickel et al.*, 1988; *Laszlo et al.*, 1995]. The mean integrated band cross section for this transition from these

[1]Department of Chemistry and Chemical Biology, Harvard Universtiy, Cambridge, Massachusetts.
[2]NOAA Aeronomy Laboratory, Boulder, Colorado.
[3]Now with the Dept. of Chemistry, University of Colorado, Boulder, Colorado.
[4]Jet Propulsion Laboratory, California Institute of Technology, Pasadena, California.

Paper number 96JD03712.
0148-0227/97/96JD-03712$09.00

studies is $2.4 \pm 0.4 \times 10^{-15}$ cm^{-1} molecule^{-1} cm^2. By scaling this value with the ratio of the Franck-Condon factors for the (4–0) and (2–0) transitions [*Rao et al.*, 1974], we obtain $1.15 \pm 0.3 \times 10^{-15}$ cm^{-1} molecule^{-1} cm^2 for the integrated (2–0) band cross section. This value agrees well (~20%) with the rotationally resolved cross sections for this band determined by *Stickel et al.* [1988].

3. Line Positions and Cross Sections of the Rotationally Resolved 2–0 Band

To determine the line positions and cross sections of the (2–0) band, a 1-m fast-flow reactor was used to produce a high concentration of IO by reacting O with I_2. Atomic oxygen was created by microwave discharge of trace O_2 in helium. The addition of ozone to the flow reactor was found to substantially increase the concentration of IO. This is presumably due to the regeneration of IO through the reaction of O_3 and I atoms produced by the reactions of IO with IO and O. Absorption due to IO was measured using a high-resolution FTS (Bruker 120). For these measurements a xenon arc lamp source, quartz beamsplitter, and spectrally filtered (Corion, S10-450) silicon photodiode detector were used.

Initially, IO spectra were obtained at low pressure (13 mbar) and high resolution (0.02 cm^{-1}). The measured line widths are consistent with the instrument width convolved with the Doppler and lifetime broadening parameters determined by *Bekooy et al.* [1983]. The wavelength scale was calibrated using line positions calculated from the molecular parameters of *Bekooy et al.* The RMS deviation of our observed line positions (Table 1) from the calculated values was only 0.00043 cm^{-1}. However, a slight trend in the difference between our measured and the calculated line positions was observed; most of the observed low-J line positions were at a slightly higher frequency than calculated, while the high-J line positions were red-shifted. Since the quoted error for *Bekooy et al.'s* observations varied from 0.0025 to 0.0031 cm^{-1}, our absolute uncertainty is also of the order of 0.003 cm^{-1}. The FWHM of the rotational transitions increases with the quantum number, due to the increasing predissociation rate of the higher rotational states; by $J = 33$ the widths exceed 0.10 cm^{-1}. Absorption measurements of IO were also obtained at higher pressures (60-250 mbar) characteristic of the lower stratosphere. These high-pressure observations were used to determine a pressure broadening coefficient of $2.7 \pm 0.5 \times 10^{-4}$ cm^{-1} mbar^{-1} for N_2.

The line positions and spectral properties of the IO lines used in this analysis are listed in Table 1. The line positions are the low-pressure values observed by us in the laboratory. The strengths of the individual rotational lines are calculated from the partition function and the Honl-London factors [*Herzberg*, 1950] normalized to a total band strength of 1.15×10^{-15} cm^{-1} molecule^{-1} cm^2. The widths are computed for stratospheric conditions: $p = 110$ mbar; $T = 210$ K. The Gaussian component is the quadratic sum of 0.0195 cm^{-1} for the thermal broadening and 0.0268 cm^{-1} for the broadening of the observed lines due to the entrance aperture of the FTS [see *Brault*, 1985]. The Lorentzian width is the sum of 0.0354 cm^{-1} for pressure broadening, $\Delta\nu = 2.7 \times 10^{-4}$ cm^{-1} mbar^{-1} $\times p \times (300\ \text{K} / T)^{1/2}$, and the natural width from *Bekooy et al.*, here represented by the formula, $\Delta\nu = 0.0044 + 0.0000916 \times J' \times (J' + 1)$ cm^{-1}, where J' is the rotational quantum number in the excited state.

Table 1. Spectral Parameters for IO

Line	Position, cm^{-1}	Intensity	Lorentzian Width, cm^{-1}	FWHM[a], cm^{-1}	Weight	Status[b]
P 26.5	22,405.463	0.067	0.102	0.112	11.39	S
P 25.5	22,409.659	0.076	0.097	0.108	12.39	S
P 24.5	22,413.719	0.085	0.093	0.104	13.40	S
R 31.5	22,416.846	0.031	0.140	0.148	7.06	S
P 23.5	22,417.639	0.096	0.088	0.100	14.40	—
R 30.5	22,420.662	0.036	0.134	0.142	7.91	S
P 22.5	22,421.423	0.106	0.084	0.096	15.37	—
R 29.5	22,424.337	0.042	0.128	0.136	8.82	S
P 21.5	22,425.069	0.117	0.080	0.093	16.30	S
R 28.5	22,427.879	0.049	0.122	0.131	9.78	S
P 20.5	22,428.577	0.129	0.076	0.089	17.17	S,W
R 27.5	22,431.280	0.056	0.117	0.126	10.79	W
P 19.5	22,431.946	0.140	0.073	0.086	17.96	S
R 26.5	22,434.541	0.064	0.112	0.121	11.82	W
P 18.5	22,435.177	0.151	0.069	0.083	18.64	S
R 25.5	22,437.665	0.073	0.107	0.117	12.88	W
P 17.5	22,438.270	0.162	0.066	0.081	19.21	W
R 24.5	22,440.652	0.082	0.102	0.112	13.95	S
P 16.5	22,441.226	0.171	0.063	0.078	19.63	S,W
R 23.5	22,443.498	0.092	0.097	0.108	15.01	S
P 15.5	22,444.043	0.180	0.060	0.076	19.90	S
R 22.5	22,446.206	0.102	0.093	0.104	16.06	O
P 14.5	22,446.723	0.187	0.058	0.074	20.00	S
R 21.5	22,448.777	0.113	0.088	0.100	17.06	S
P 13.5	22,449.264	0.192	0.055	0.071	19.90	S
R 20.5	22,451.210	0.125	0.084	0.096	18.01	—
P 12.5	22,451.668	0.195	0.053	0.070	19.60	—
R 19.5	22,453.503	0.136	0.080	0.093	18.88	W
P 11.5	22,453.933	0.196	0.051	0.068	19.08	W
R 18.5	22,455.659	0.147	0.076	0.089	19.65	S
P 10.5	22,456.061	0.194	0.049	0.066	18.35	—
R 17.5	22,457.676	0.158	0.073	0.086	20.31	S
P 9.5	22,458.050	0.188	0.047	0.065	17.40	S
R 16.5	22,459.555	0.169	0.069	0.083	20.83	—
P 8.5	22,459.901	0.180	0.046	0.068	16.22	—
R 15.5	22,461.296	0.178	0.066	0.081	21.20	S
P 7.5	22,461.615	0.168	0.044	0.063	14.83	—
R 14.5	22,462.898	0.187	0.063	0.078	21.39	S
P 6.5	22,463.190	0.152	0.043	0.062	13.23	S
R 13.5	22,464.363	0.193	0.060	0.076	21.39	S
P 5.5	22,464.627	0.134	0.042	0.061	11.43	—
R 12.5	22,465.687	0.198	0.058	0.074	21.18	—
P 4.5	22,465.926	0.112	0.041	0.060	9.43	—
R 11.5	22,466.876	0.201	0.055	0.071	20.77	—
P 3.5	22,467.087	0.087	0.041	0.060	7.23	—
R 10.5	22,467.926	0.201	0.053	0.070	20.13	W
P 2.5	22,468.096	0.053	0.040	0.060	4.40	W
R 9.5	22,468.837	0.198	0.051	0.068	19.27	—
R 8.5	22,469.610	0.192	0.049	0.066	18.18	S,W
R 7.5	22,470.245	0.183	0.047	0.065	16.88	S,W
R 6.5	22,470.742	0.170	0.046	0.064	15.36	—
R 5.5	22,471.101	0.154	0.044	0.063	13.63	Bl
R 4.5	22,471.324	0.135	0.043	0.062	11.72	Bl
R 3.5	22,471.404	0.113	0.042	0.061	9.63	Bl

Pressure, 110 mbar; Temperature, 210 K; Gaussian width, 0.033 cm^{-1}
[a]FWHM, Full Width at Half Maximum, cm^{-1}
[b]Status: W, Water interference; S, Solar interference; Bl, Blend; O, Other absorption feature; —, Used in Analysis

4. Atmospheric Column Measurements

Solar spectra in the vicinity of the IO transitions were recorded for three sunrises during March 1995 (see Table 2). Poor viewing conditions limited the number of observations. Only one sunset measurement was obtained, and, unfortunately,

Table 2. Kitt Peak Observations

	Time, MST	SZA[a], deg	Refraction, arcsec	Wavelength Correction[b], (x 10^6)	Signal / Noise due to shot noise
	March 3, 1995				
Begin	7:04:17	88.186	853.5	–0.122	
End	7:16:27	85.643	505.0	–0.132	1300
Begin	9:25:22	60.132	72.9	–0.446	
End	9:48:42	56.009	61.3	–0.539	6500
	March 4, 1995				
Begin	7:02:41	88.271	871.0	–0.129	
End	7:12.49	86.149	552.5	–0.136	1300
Begin	8:53:41	65.765	94.5	–0.343	
End	9:40:35	57.108	64.1	–0.514	9000
	March 13, 1995				
Begin	6:50: 6	88.583	937.0	–0.225	
End	6:56.56	87.138	667.9	–0.228	1300
Begin	8.56:49	62.517	80.6	–0.464	
End	9:29:35	56.272	61.6	–0.583	7500

[a]True solar zenith angle (not corrected for refraction)
[b]Fractional shift (Doppler) of the solar spectrum due to relative Earth–Sun velocity changes.

it has considerably poorer signal-to-noise ratio (S/N) than the sunrise data and is not used further in this analysis. Like at other mountaintop observatories, the height of the planetary boundary layer grows during the day, leading to significantly larger residuals. For instance, the H_2O column for the sunset data is nearly twice as large as the sunrise columns. Aircraft-, satellite-, or balloon-borne observations would be useful for removing this influence of the planetary boundary layer.

The spectra were taken at the center of the 80 cm solar image of the McMath-Pierce Solar Telescope of the National Solar Observatory (near Tucson, Arizona), using the solar FTS described by *Brault* [1978] with a 1-cm-diameter aperture. The telescope and spectrometer used here have a long history of obtaining measurements of weak atmospheric absorption spectra using high air mass observations, including the first detection of weak quadrupole transitions in molecular oxygen [*Brault*, 1980] and nitrogen [*Camy-Peyret et al.*, 1981], as well as the earliest high-resolution work on H_2O below 600 nm [*Rothman*, 1978]. When used in the visible, this instrument has a limiting resolution of 0.01 cm^{-1} (0.0002 nm at 445 nm). For these pressure-broadened atmospheric spectra, the resolution was decreased to 0.053 cm^{-1} (0.5 / maximum optical path difference) to maximize the S/N. With the band pass defined by a 20-nm interference filter centered at 445 nm, the S/N due to shot noise was 6500 to 9000 for the low air mass spectra (SZA ≈ 60°, 8 to 20 double-sided scans, 125 s/scan) and 1300 for the high air mass spectra (SZA ≈ 88°, 3 to 5 double-sided scans). The shot noise is determined by measuring the root mean square (RMS) noise in the baseline just outside the 20-nm filter band pass, normalized to the intensity at ν = 22,460 cm^{-1}.

5. Wavelength Calibration

An accurate wavelength scale is essential to a proper analysis, since the IO spectrum must be aligned with the atmospheric spectrum to high accuracy (0.01 cm^{-1}). The raw wavenumber scale for Fourier transform spectrometers is referenced to the exact wavelength of a reference laser (typically a He-Ne); however, errors in the absolute wavelength calibration can occur in a number of ways. An error is introduced if the reference laser and sample beams are not parallel. For example, if the laser beam is on axis but the mean sample beam is off by 1 mrad, the scale will be shifted by 5×10^{-7}. A further shift is caused by the finite size of the aperture, which places some rays off axis even if the center of the field is on axis. Since the laser wavenumber may drift slowly and the wavelength scale is sensitive to the alignment, the usual method for determining the absolute frequency is to use internal standards; that is, known spectral features that share a common angular aperture and integration time. We have chosen the photographic observations of *Pierce and Breckinridge* [1974] at the Sun center for standards that in turn were calibrated using interferometrically measured thorium lines as references. We selected 67 solar lines of moderate strength and good symmetry, whose positions are known to within 0.001 cm^{-1}. The positions were then corrected for the relative Earth-Sun velocity at the time of observation. This correction was near zero for the high air mass sunrise observations, about 0.01 cm^{-1} for the low air mass sunrise spectra, and just over 0.06 cm^{-1} at sunset, with negligible uncertainty due to the accuracy of our knowledge of Earth's motion with respect to the Sun. The uncertainty in the wavenumber calibration factor using all 67 lines was typically 1.3×10^{-8} (0.0003 cm^{-1} or 0.000006 nm in this region), which is consistent with the uncertainties in the Pierce and Breckinridge values. The spectral positions obtained during four high Sun measurements showed a very high degree of internal consistency (typically 0.00024 cm^{-1} for each individual line) but had a standard deviation of 0.0024 cm^{-1} from the individual Pierce and Breckinridge values, indicating the presence of a systematic error. This error is most probably in the photographic measures, which showed an order of magnitude higher scatter as well. In any event, the derived wavelength calibration is more than adequate for present purposes.

6. IO Slant Column

Shown in Plate 1a are small portions of the normalized solar spectra obtained at both high and low air mass on the morning of March 3, 1995. The solar intensity varies considerably due to

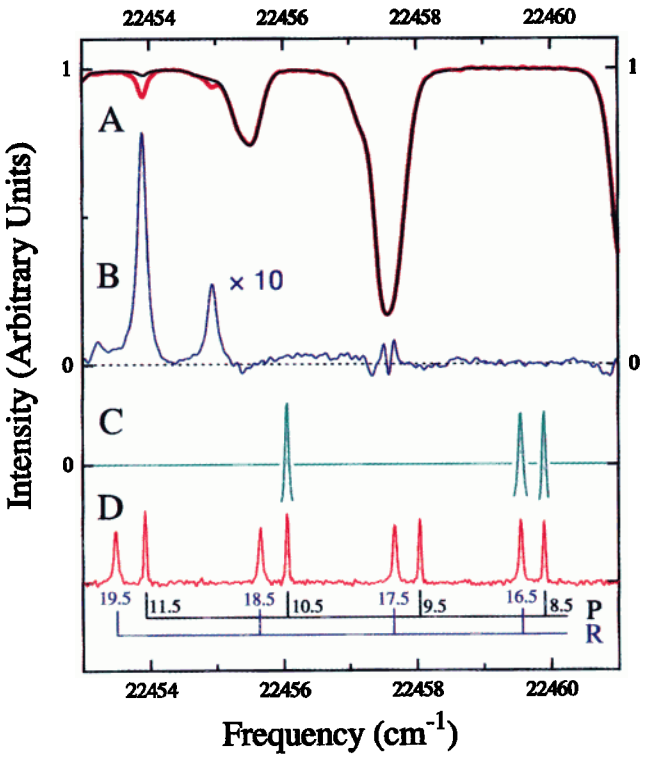

Plate 1. Solar absorption spectroscopy and atmospheric iodine monoxide. (a) A small portion of the normalized solar spectrum near 22,460 cm^{-1} (445 nm) taken just after sunrise (red) and later at low air mass (black). The spectra were taken with the Fourier transform spectrometer on the McMath-Pierce Solar Telescope, Kitt Peak, Arizona. (b) The absorbance (×10) derived from the ratio of the high air mass and low air mass spectra. Large absorption features (> 2%) due to water vapor are seen. The noise in the absorbance is larger near the solar Fraunhofer lines. Absorption due to atmospheric NO_2 has been removed. (c) A series of local, differential cross sections for the IO lines selected in this region (a portion of the "gap" function). The cross correlation of the gap function with the residual (Plate1b) is used to determine the atmospheric IO signal. Fifteen rotational IO lines that are more than 0.45 cm^{-1} away from water or Fraunhofer features are used in the analysis. (d) Eight of the rotational features of IO in the *A–X* (2,0) band (P, and R branches). This absorbance spectrum was taken in the laboratory with a Fourier transform spectrometer. Broadening increases with rotational quanta due to the increasing predissociation of the excited state.

the absorption in the solar atmosphere (the Fraunhofer lines). Large absorption features due to telluric water vapor are also seen in the absorbance spectrum shown in Plate 1b. Furthermore, as is evident in the expanded section shown in Plate 2, numerous small features due to NO_2 are present in both the high and low air mass spectra with strengths roughly proportional to the ratio of the stratospheric air mass (× 9). In Plate 2b we have removed the contribution due to NO_2. An NO_2 spectrum taken in the laboratory at low temperature (–35 °C) and low pressure (< 15 mbar) was used for removing the influence of NO_2. The procedure used is discussed in the Appendix.

In Plate 2b, we also show what would be observed if we added a stratospheric IO column of 2.7×10^{13} molecule cm^{-2} to the high air mass spectrum and 0.4×10^{13} molecule cm^{-2} to the spectrum taken at SZA = 60°. As discussed below, these are the expected slant columns, assuming that 1 pptv of total inorganic iodine is present in the stratosphere. Clearly, the abundance of stratospheric iodine is not very large (< 0.5 pptv), since no absorption features due to IO are present in these unratioed spectra at even 50% of the depths illustrated.

A more precise estimate for the IO column can be achieved by using more of the lines in the IO (2–0) band. The solar spectrum in the region shown in Plate 2 is remarkably quiet; there are no H_2O or solar Fraunhofer lines. To make use of the entire band of IO, we first use the low air mass spectrum to normalize for the variation in solar intensity. In principle, the ratio of the high air mass to low air mass spectrum yields the atmospheric transmittance of the air mass difference. However, because the relative Earth-Sun velocity changes between the times of the two observations, the solar lines are slightly shifted (~0.005 to 0.010 cm^{-1}), while the atmospheric lines remain fixed. Nevertheless, for optically thin absorption features, the ratio works well because the shift is much smaller than the atmospheric line widths and the two records exhibit large differences in atmospheric absorption. Under these conditions, the most precise results are obtained by lining up the two spectra for best cancellation of the strong solar features. The alignment is sensitive to about 0.0005 cm^{-1} (equivalent to a Doppler shift of ~6 m/s), limited by variations in the positions of the individual Fraunhofer lines, possibly due to depth-dependent solar mass motions.

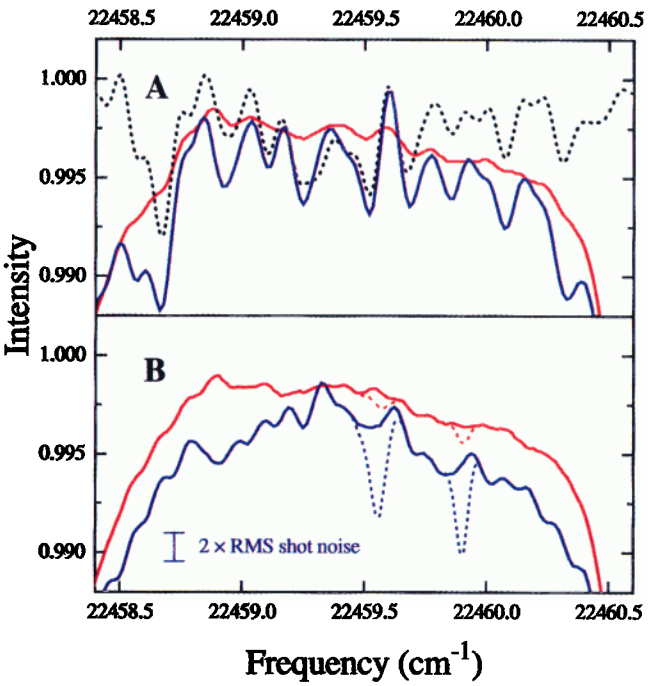

Plate 2. The solar spectrum near 22,459.5 cm^{-1} is free of solar or telluric water lines. In red, the solar spectrum at solar zenith angle (SZA) = 60° and in blue at 88° taken on March 3, 1994, are shown. (a) Absorption due to stratospheric NO_2 is clearly observed in both the high and low air mass spectra. Shown as a dotted black line is the NO_2 absorption spectrum taken in the laboratory at low temperature (240 K) and low pressure (8 mbar). (b) After removing the signature due to NO_2, the residuals are very small – close to the shot noise limit for the instrument (see Table 2). The dotted lines show the absorption expected if 1 pptv of inorganic iodine was present in the stratosphere.

After dividing the high air mass spectra by the low air mass spectra and removing the NO_2 signal (see Appendix), we obtain the residual absorption which is used to determine the IO slant column (Plate 1b). Of the many rotational lines of IO listed in Table 1, 15 are used for the determination of column abundance from the ratio of low Sun to high Sun spectra. A line is eliminated from the analysis if (1) it is within ±0.45 cm^{-1} of a water vapor line (marked W in Table 1) or other absorption feature (marked O in Table 1), (2) it is within ±0.45 cm^{-1} of a strong solar line and thus contaminated by errors in the ratio (marked S), (3) it is blended with another IO line near the band head (Bl), or (4) it has low intensity.

If the residual in the high Sun/low Sun ratio consisted only of IO absorption plus random noise, we could evaluate the contribution of the remaining IO lines (marked with a dash in Table 1) using a cross-correlation technique [cf. *Larson et al.*, 1977]. However, because the spectrum is still subject to possible interference from solar residuals and H_2O (and other unknown) lines, we use a similar technique that allows us to view the contributions of the individual lines. For example, R(22.5) is eliminated due to the presence of an absorption feature of unknown origin 0.3 cm^{-1} to the blue of this line. For each of the IO lines a Voigt function is constructed using the parameters in Table 1 and truncated outside a region 2.75 times the FWHM. The mean value inside the region is then subtracted, leaving a differential cross section for the line (see Plate 1c), which we call the IO "gap function." For the nth line, the contribution to absorbance by IO, c_n, is evaluated as the sum (over the frequencies covering each line) of the product of the gap function, g_n, and the observed absorbance, a_n, divided by the sum of the squares of the gap function:

$$c_n = \Sigma(a_n \times g_n) / \Sigma(g_n \times g_n).$$

If we write a_n more generally as $a_n = k_n \times g_n + \varepsilon$, where k is the total observed band intensity (summed over the n rotational lines) and ε represents a noise contribution with $\Sigma(\varepsilon \times g_n) \approx 0$, then $c_n \approx k_n$. This result is insensitive to any constant offset (since the mean of the gap function is zero) and to any linear slope in the region (since the gap function is symmetric). We thus obtain from each line a separate estimate of the value of k. These values are then used to obtain a weighted mean (with a weight for each k_n that is proportional to the square of the strength of that line, assuming uniform noise) and an estimate of the variance. For an integrated band cross section of 1.1×10^{-15} cm^{-1} $molecule^{-1}$ cm^2, a value of $k = 1$ cm^{-1} corresponds to 9×10^{14} molecule cm^{-2} in the path.

To obtain an estimate of the uncertainty in the result and to check for any possible systematic effects, this process is repeated after shifting the gap function away from its proper alignment by ±0.45 cm^{-1}, or roughly 12 line widths (a cross correlation). The results are shown in Plate 3a for each of the three sunrise observations (black) and the average (red), which is also shown in Plates 3c and 3d. Note the small peak near 0.0 cm^{-1} lag, indicating a marginal detection of IO (the zero lag position in Plate 3 has an uncertainty of approximately 0.003 cm^{-1}). From this analysis, we determine that the IO signal observed for these three sunrise observations is 0.0045 ± 0.0045 cm^{-1}. The uncertainty (2σ) is determined from the peak-to-peak noise in the offset signals.

Shown in Plate 3b (blue) is the expected response for a 4×10^{12} molecule cm^{-2} change in the IO slant column between 88° and 60° SZA and corresponding to the average signal shown in Plate 3a. To show this graphically, in Plate 3c we have subtracted a stratospheric column change (centered at 110 mbar) of 4.0 (blue), 0.0 (red), and 8.0×10^{12} (black) molecule cm^{-2}, representing the mean and the lower and upper limits to the column change.

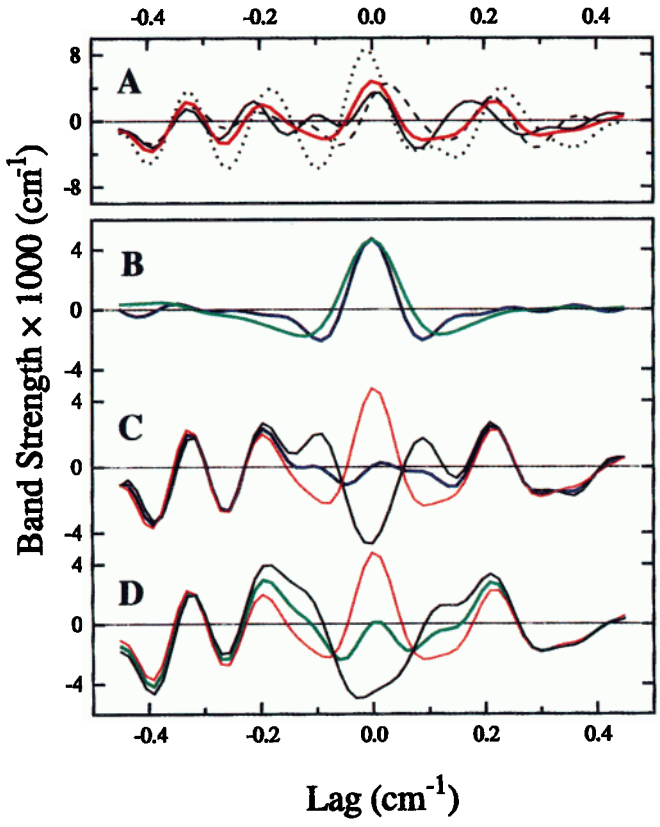

Plate 3. IO Signal. (a) The IO band strength is derived from the cross correlation of the "gap" function (Plate 1c) and the atmospheric absorption (Plate 1b) for three sunrise observations; the average is shown in red. Fifteen IO rotation lines are used in this analysis. (b) Expected signal for a 2×10^{13} molecule cm^{-2} change in the stratospheric IO column (blue) or for a 1×10^{14} change in tropospheric IO assumed to be centered at 500 mbar (green). A value of 1 cm^{-1} (at 0.0 cm^{-1} lag) corresponds to a stratospheric IO column of 9×10^{14} molecule cm^{-2} in the path. The absolute frequencies are known to better than 0.003 cm^{-1}. (c) The mean of the three sunrise observations (red) and the signal after subtraction of a stratospheric IO slant column equal to 4×10^{12} (blue) and 8×10^{12} (black) molecule cm^{-2}. (d) The mean of the three sunrise observations (red) and the signal after subtraction of a tropospheric IO slant column equal to 2×10^{13} (green) and 4×10^{13} (black) molecule cm^{-2}.

This analysis produces an estimate of the change in the slant column of IO between 88° and 60° SZA. To infer the mixing ratio of stratospheric iodine from this measurement, we need to estimate how stratospheric iodine is partitioned between the various iodine containing species both as a function of altitude and solar zenith angle. This is discussed in detail below. In addition, however, we need to consider the potential influence of iodine present in the troposphere.

Our sensitivity to tropospheric IO is considerably smaller than for IO present in the stratosphere, due to the pressure broadening of the spectral lines and our use of the gap filter (see Appendix).

To illustrate how much tropospheric IO would be required to fully explain the observed IO signal, in Plate 3d we subtract a tropospheric column change of 0.0 (red), 2.0 (green), and 4.0 × 10^{13} (black) molecule cm^{-2} of IO from the cross correlation of the gap filter with the atmospheric transmittance, assuming the IO column is centered at 500 mbar (265 K) and that no iodine is present in the stratosphere. A column change 5 times larger would be required to produce the IO signal observed if it is weighted at 500 mbar rather than 100 mbar. Our sensitivity to tropospheric IO decreases even more rapidly with pressure above 500 mbar. For instance, to produce the signal seen in Plate 3a the tropospheric column change would have to be approximately 15 times larger (6 × 10^{13} molecule cm^{-2}) if it was centered in the planetary boundary layer.

Despite the reduced sensitivity to tropospheric IO, iodine present in the lower atmosphere could lead to either an overestimation or underestimation of the stratospheric column. If the slant column of tropospheric IO is larger at SZA 88° than 60°, then our estimate of the stratospheric column is too high. On the other hand, because the photolysis rates of the inorganic iodine reservoir species (e.g., $IONO_2$, HOI) will be considerably smaller at high SZA in the troposphere than in the stratosphere, there is a small possibility that the tropospheric IO slant column could be larger at 60° than at 88°, despite the much larger air mass (9 times), thus leading to an underestimation of the stratospheric column. However, as shown in Plate 2, the low air mass spectrum (red) has very little structure at the appropriate frequency width (≈0.1 cm^{-1}). Because there are no obvious absorption features coincident with the IO wavelengths, we are assured that by using the low air mass spectrum to remove the solar structure we are not adding significant signal due to absorption by IO of either sign to the atmospheric transmittance. Additionally, the signal-to-noise ratio of the low zenith angle spectrum is sufficiently high that it does not contribute to the final uncertainty. For example, in the region shown in Plate 2b, twice the RMS noise at 0.1 cm^{-1} frequency width is less than 0.0004 absorption, essentially shot noise limited (see Table 2). For the IO lines used in this analysis, the absorption cross sections are approximately 2 × 10^{-16} cm^2 and so this noise is equivalent to a stratospheric IO column of less than 2 × 10^{12} molecule cm^{-2}.

Three conclusions can be drawn from the results of Plate 3a: (1) The direct detected IO signal is very small (equivalent to a stratospheric IO slant column decrease of 4 ± 4 × 10^{12} molecule cm^{-2} as SZA changes from 88° to 60°); (2) Because there is considerable agreement between the different observations, the curves represent a systematic signal rather than random noise; (3) However, because Plates 3c and 3d are similar, we can not be sure whether the observed absorption is due to a stratospheric or a larger tropospheric IO slant column change. Additionally, because the low air mass spectrum could contain a small tropospheric IO slant column that is not present early in the morning, the stratospheric IO slant column change could be systematically low by no more than 2 × 10^{12} molecule cm^{-2}, as determined from the RMS noise in the low SZA spectra. Thus we conclude that the stratospheric IO column changed by no more than 4 (+6 –4) × 10^{12} molecule cm^{-2} between 88° and 60° SZA in the morning (2σ). The upper limit, 1 × 10^{13} molecule cm^{-2}, is very conservative; such a stratospheric IO column would produce absorption features approximately 1/2 the depth of those illustrated by the dotted line in Plate 2b. No such features are observed.

7. Mixing Ratio of Stratospheric Iodine

To infer the total inorganic iodine mixing ratio from the IO slant column change, we use a photochemical model to calculate the slant column of IO between an observer at Kitt Peak and the Sun as a function of SZA for a variety of assumptions concerning the partitioning of iodine species. The concentration of the inorganic iodine species IO, I, $IONO_2$, HI, and HOI are computed as a function of time, at a series of altitudes, assuming each gas reaches a balance between production and loss over a 24-hour period. Details of the photochemical model are provided elsewhere [*Salawitch et al.*, 1988, 1994a,b]. Iodine chemistry in the model has been updated with the most recent laboratory measurements (Table 3). The model is constrained by profiles of temperature and aerosols based on observations from the National Meteorological Center and the Stratospheric Aerosol and Gas Experiment II [*McCormick et al.*, 1989], respectively. Profiles of O_3 are derived from a climatology based on the Middle Atmosphere Program compendium of satellite observations [*Keating and Young*, 1985] and in situ measurements of O_3 in the lower stratosphere, described by *Salawitch et al.* [1994a,b]. Profiles of other long-lived precursors of reactive gases, such as H_2O, CH_4, N_2O, and NO_y, are specified primarily from atmospheric trace molecule spectroscopy observations [*Gunson et al.*, 1990]. Profiles of inorganic bromine (Br_y) and chlorine (Cl_y) are specified based on their observed correlation with N_2O [*Schauffler et al.*, 1993; *Woodbridge et al.*, 1995]. Model inputs for pressure, temperature, N_2O, and radical precursors are given in Table 4. The calculated concentrations of the free radicals at solar noon are given in Table 5. This model has been tested extensively against observations of HO_x, NO_x, and ClO in the lower stratosphere (between the tropopause and ~21 km), and, in general, describes the observations to within their 2σ uncertainties (±50, ±20, ±30%, respectively) [*Salawitch et al.*, 1994a,b; *Keim et al.*, 1996; *Gao et al.*, 1997]. The model has also been tested with observations of HO_x, NO_x, and ClO in the

Table 3. Additions and Changes From JPL 94[a] to Iodine Chemistry Used in the Model.

Reaction	Value Used	Reference
$O + IO \rightarrow O_2 + I$	1.2×10^{-10} cm^3 s^{-1}	Laszlo *et al.*, 1995
$IO + ClO \rightarrow$ products	$5.1 \times 10^{-12} \exp(280/T)$ cm^3 s^{-1}	Turnipseed *et al.*,1995b
$IO + BrO \rightarrow$ products	$2.2 \times 10^{-11} \exp(270/T)$ cm^3 s^{-1}	Laszlo *et al.*, 1997 Turnipseed *et al.*,1995b
$IO + NO \rightarrow I + NO_2$	$1.0 \times 10^{-11} \exp(185/T)$ cm^3 s^{-1}	Turnipseed *et al.*,1995a
$IO + h\nu \rightarrow I + O$		Laszlo *et al.*, 1995
$IONO_2 + h\nu \rightarrow$ products	$\sigma_{IONO_2} = \sigma_{BrONO_2}$ red shifted 50 nm.	Atkinson *et al.*, 1992
$HOI + h\nu \rightarrow OH + I$		Atkinson *et al.*, 1992

[a] *DeMore et al.* [1994]

Table 4. Model Inputs

Z, km	T, K	P, mbar	O_3, ppmv	N_2O, ppbv	NO_y, ppbv	Cl_y, ppbv	Br_y, pptv	H_2O, ppmv	CH_4, ppmv
12	211.9	198.3	0.14	307	0.40	0.18	1.11	3.82	1.69
14	211.3	143.8	0.31	302	0.76	0.27	2.12	3.86	1.67
16	208.6	104.0	0.44	297	1.13	0.35	3.10	3.90	1.65
18	205.8	74.9	0.98	292	1.50	0.44	4.05	3.94	1.63
20	207.1	53.9	1.96	287	1.87	0.53	4.98	3.98	1.61
22	218.8	38.9	3.29	258	4.04	1.02	9.87	4.22	1.50
24	211.0	28.2	4.69	229	6.20	1.48	13.80	4.45	1.38
26	214.4	20.5	5.91	200	8.37	1.91	16.90	4.68	1.26
28	218.8	15.0	6.82	171	10.50	2.28	19.00	4.92	1.15
30	224.7	11.0	7.62	142	12.70	2.60	20.30	5.16	1.03

Abbreviations: ppmv, parts per million by volume; ppbv, parts per billion by volume; pptv, parts per trillion by volume. The mixing ratio of inorganic iodine is assumed to be constant with altitude (see text).

mid and upper stratosphere [e.g., *Chance et al.*, 1996]. Although observations of BrO are more limited [e.g., *Brune et al.*, 1988; *Avallone et al.*, 1995; *Arpag et al.*, 1994; *Fish et al.*, 1995], the measurements suggest that our understanding of the concentration and partitioning of Br_y is accurate enough for the purposes of this study.

The mixing ratio of inorganic iodine is assumed to be constant with altitude above the tropopause. This approximation is valid provided there are no sinks of inorganic iodine in the stratosphere and the mixing ratio of the iodine containing gases entering the stratosphere through the tropical tropopause and through the subtropical jet (into the so-called middle world) are similar. The organic iodine source gases, such as methyl iodide, will be converted to inorganic form within a few days of entering the stratosphere. We assume that no IO is present in the troposphere above Kitt Peak during the period of these observations. The tropopause height is assumed to be 200 mbar, based on temperatures from the NASA Goddard Space Flight Center data assimilation model (Paul Newman, private communication, 1995) and radiosonde measurements near Tucson, Arizona, for the days of observation. Reaction rate coefficients and absorption cross sections are from *DeMore et al.* [1994], except where noted in Table 3. Rapid photolysis rates for INO and INO_2 preclude these species from being important reservoirs of inorganic iodine during daylight.

The calculated change in the vertical and slant column abundance of stratospheric IO as a function of SZA, assuming a total iodine mixing ratio of 1 pptv, is shown in Figure 1a. The slant column of IO is computed for an observer at 2.1 km, taking into account variations of IO with altitude and SZA along the path to the Sun [*Salawitch et al.*, 1988]. Accurate simulations of the change in concentration of NO, NO_2, and ClO at sunrise and sunset observed during the Stratospheric Photochemistry, Aerosols, and Dynamics Experiment lead to confidence in the accuracy of the computed photolysis rates at high SZA [*Salawitch et al.*, 1994a]. Approximately 1/3 of the change in the column is contributed by iodine in the lowest part of the stratosphere (between the tropopause and 380 K potential temperature).

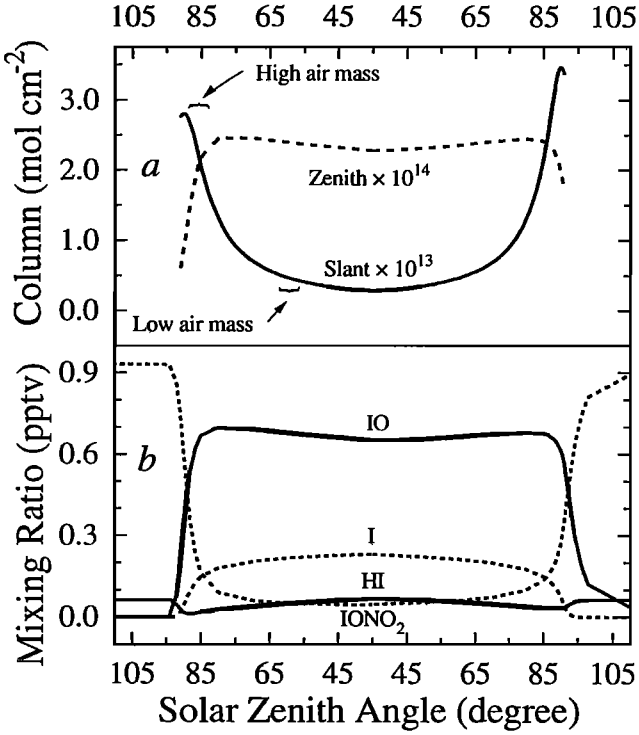

Figure 1. Inorganic iodine and the IO slant column. A photochemical model is used to relate the total inorganic iodine mixing ratio to the change in the IO slant column with SZA. The concentration of the inorganic iodine species IO, I, $IONO_2$, HI, and HOI are computed as a function of time and altitude assuming each gas reaches a balance between production and loss over a 24–hour period. (a) Computed slant and vertical columns of IO as a function of SZA, assuming the mixing ratio of total inorganic iodine = 1 pptv at all altitudes above the tropopause (200 mbar). Plate 2b illustrates the IO line depths that would be observed for slant columns of IO as large as shown here. (b) Calculated diurnal variation of various iodine-containing species at 20 km.

Figure 1b illustrates the calculated diurnal variation of the inorganic iodine species at 20 km for a total inorganic iodine reservoir of 1 pptv. The mixing ratio of IO is predicted to increase rapidly at sunrise due to the photolysis of $IONO_2$, the dominant nighttime reservoir. The small asymmetry between morning and evening concentrations of IO is due to the rather slow photolysis rate of $IONO_2$. The absorption cross sections for $IONO_2$ are uncertain, however. For the calculations shown in Figure 1, the photolysis rate of $IONO_2$ is estimated by shifting the $BrONO_2$ cross sections to the red by 50 nm, consistent with the recommendation of *Atkinson et al.* [1992] and with preliminary laboratory measurements by *Barnes et al.* [1991]. Unlike the other halogen families, a significant fraction of inorganic iodine exists

Table 5. Calculated Radical Concentrations at Local Noon

Z, km	NO, pptv	NO_2, pptv	OH, pptv	HO_2, pptv	ClO, pptv	BrO, pptv	IO[a], pptv
12	58.5	11.4	0.16	2.00	0.18	0.41	0.08
14	77.6	23.9	0.27	2.42	0.97	0.93	0.10
16	131.	39.6	0.43	2.51	1.99	1.50	0.10
18	137.	63.4	0.64	4.25	8.04	1.94	0.12
20	141.	101.	1.01	8.52	26.1	2.18	0.13
22	306.	292.	1.82	13.00	65.8	4.03	0.13
24	627.	664.	3.39	20.10	111.	5.34	0.13
26	1280.	1350.	6.46	29.70	161.	6.45	0.13
28	2380.	2380.	12.1	42.00	232.	7.54	0.13
30	3880.	3640.	21.8	59.60	342.	8.49	0.12

[a]The mixing ratio of inorganic iodine is assumed to be 0.2 pptv (see text).

in atomic form due to the rapid photolysis rate of IO. The simulations shown in Figure 1 use absorption cross sections for IO measured by *Laszlo et al.* [1995], which lead to faster photolysis rates than calculated using the cross sections recommended by *Atkinson et al.* [1992] because of the existence of a large continuum near 390 nm. The cross sections of *Laszlo et al.* [1995] are consistent with theoretical calculations of the Franck-Condon factors by *Rao et al.* [1974] and recent measurements by *Himmelmann et al.* [1996].

The computed slant column of IO is insensitive to assumptions for a variety of kinetic parameters. We have performed a series of calculations using rates and cross sections identical to those used above, except for the parameter in question. The computed change in the slant column of IO between mid-day and the terminator for each calculation is compared to results shown in Figure 1a. If the absorption cross-sections for $IONO_2$ are identical to those for $BrONO_2$ (likely a lower limit), the change in slant column of IO between midday and the morning terminator is reduced 50% and the change in slant column between midday and the evening terminator is reduced 25%. Allowing for the hydrolysis of $IONO_2$ to HOI on sulfate aerosol at a rate similar to that observed for $BrONO_2$ ($\gamma = 0.8$) [*Hanson et al.*, 1996] results in a slight increase (~10%) in the change in slant column and greatly reduces the sensitivity to assumptions about the photolysis rate for $IONO_2$ because HOI becomes the principle inorganic iodine species at sunrise. Finally, using the cross sections for IO suggested *by Atkinson et al.* [1992] leads to a 20% increase in the change in the slant column.

The simulations shown in Figure 1a reveal that the slant column abundance of IO should change by approximately 2×10^{13} molecule cm^{-2} as the SZA varies from 60° to 88° for each pptv of inorganic iodine in the stratosphere. The expected signal due to such a column of IO is shown in Plate 2b; clearly, the stratosphere mixing ratio of IO is significantly smaller. The measured change in the slant column of IO, 4×10^{12} molecule cm^{-2}, is broadly consistent with a mixing ratio for total stratospheric iodine of 0.2 pptv. This estimate is somewhat low if the upper tropospheric air entering the middle world has a significantly smaller iodine mixing ratio than the air entering through the tropical tropopause. As an upper limit, if no iodine is present below 15 km (380 K), the mixing ratio above would be 0.3 ppt. On the other hand, if some of the observed slant column change is due to tropospheric IO, then our estimate of stratospheric IO is too high.

The small upper limit for stratospheric iodine determined in this study is corroborated by a recent study of solar spectra measured on a balloon-borne instrument. *Pundt et al.* [1997] have examined data obtained from nine flights at both high latitudes and mid latitudes. No signature attributable to absorption by five vibrational bands of IO (405–430 nm) was seen in any of the spectra. From the signal-to-noise ratio of these measurements, *Pundt et al.* [1997] determined an upper limit of 0.2 pptv total iodine at and below 20 km.

Davis et al. [1996] have recently reported measurements of methyl iodide (CH_3I) in the lower-tropical and mid-tropical troposphere. The concentration of CH_3I averaged 0.6 (+0.6 –0.3) pptv in the tropical marine boundary layer and 0.15 (+0.15 – 0.07) pptv at 10 km (~1 scale height below the tropical tropopause). Davis *et al.* suggest that the concentration of inorganic iodine could be as much as 0.5 pptv at 10 km from the photolysis of CH_3I alone. However, the authors note the very large uncertainty associated with the model used to infer the concentration of inorganic iodine from the concentration of CH_3I. In particular, they note that a small aerosol sink in the mid-troposphere could remove essentially all the inorganic iodine. Although IO and atomic iodine are expected to dominate the daytime inorganic iodine budget, potential heterogeneous chemistry of these species was not included in the model of *Davis et al.* [1996]. In any case, the small inorganic mixing ratio inferred from our and *Pundt et al.*'s measurements suggests that either very little inorganic or organic iodine reaches the stratosphere or else, once in the stratosphere, it is removed onto the sulfate aerosol.

8. Iodine and Stratospheric Ozone

The change in the slant column of IO determined here, combined with recent kinetic measurements, show that iodine chemistry does not play an important role in the photochemistry of stratospheric O_3. The IO column change is nearly 50 times smaller than measurements of the slant column of BrO [*Arpag et al.*, 1994; *Fish et al.*, 1995]. For IO to contribute significantly to ozone loss compared with BrO, the rate constants for catalytic ozone removal involving IO (e.g., IO + BrO, ClO, HO_2, and O) would have to be substantially faster than the rate constants for the equivalent reactions involving BrO. Recent measurements have greatly expanded the kinetic database for reactions involving IO [*Laszlo et al.*, 1995, 1997; *Turnipseed et al.*, 1995a,b] (See Table 3). Although the rate of IO with BrO is 20 times faster than the self reaction of BrO (a minor component of the total loss of O_3 due to bromine), the rate constants for the catalytic reactions of IO with O, HO_2, and ClO are only a factor of 2

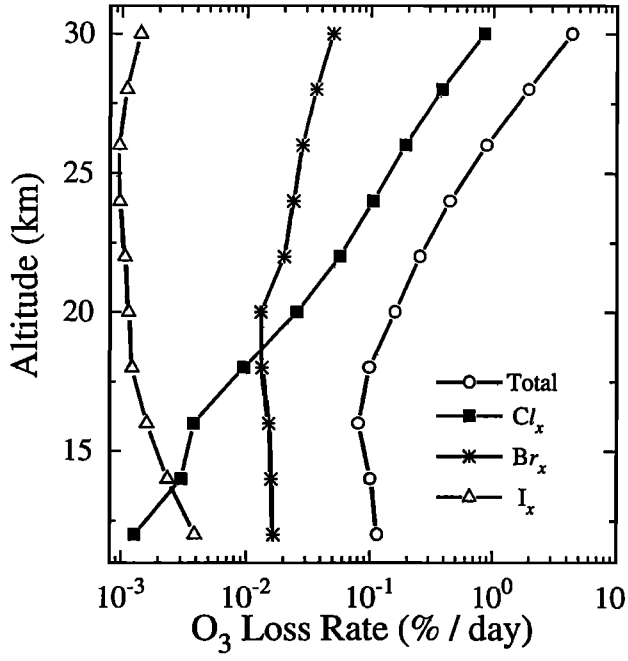

Figure 2. The removal rate of ozone. Calculated chemical destruction of ozone by halogens and the total loss due to all chemical mechanisms for March 1995. Inorganic iodine is assumed to be present at 0.2 pptv, the mixing ratio estimated in this work. The sum of all the ozone loss mechanisms due to iodine account for an ozone removal time constant of longer than 30 years. Even at the upper limit for inorganic iodine determined in this study, 0.5 pptv, the ozone removal time constant is longer than 50 years at and above 15 km where the vast majority of the stratospheric ozone column resides.

faster than the equivalent rate constants for the reactions involving BrO. A significant fraction (20–40%) of the ozone loss attributable to iodine is due to the reaction of IO with BrO. At 220 K, the rate constant for this reaction is 3.5 times larger than the rate constant for ClO + BrO. The net rate of ozone loss due to the reaction of IO with BrO will, however, depend on what products are formed. If OIO or OBrO are formed, analogous to the formation of OClO in the reaction of ClO with BrO, the net ozone loss may be slower than the total rate (depending on the photolysis products of OIO and OBrO). As an upper limit, we have assumed 100% ozone loss efficiency for the reaction of IO with BrO.

To illustrate the role of iodine reactions on the photochemistry of O_3, we have computed the diurnally averaged rates for destruction of ozone by the major catalytic cycles assuming inorganic iodine is present at 0.2 pptv at all altitudes in the stratosphere. In Figure 2, we show the calculated O_3 loss rates for all cycles involving IO with the loss rates by other halogenated cycles, as well as the total O_3 loss rate. I_x refers to all reactions involving iodine; Br_x refers to all reactions involving bromine except BrO + IO; Cl_x refers to all reactions involving chlorine except those included in I_x and Br_x. Our computed loss rate due to iodine chemistry is more than an order of magnitude slower than the rate calculated by *Solomon et al.* [1994b] in their base case because the abundance of total iodine is a factor of 5 less than they assumed and the rate constant for the reaction of IO with ClO is 5 times slower [*Turnipseed et al.*, 1995b] than they used. Our conclusions regarding the removal rate of ozone by iodine are insensitive to assumptions concerning the proscribed profiles of radical precursors. Calculations constrained by profiles of O_3, NO_y, Cl_y, and Br_y shifted vertically by ±4 km with respect to the profiles given in Table 4 yield results similar to those shown in Figure 2. Calculations constrained with the same precursor concentrations given in Table 4, but with 2 pptv of Br_y added at all altitudes (such as might occur if 2 pptv of a short-lived bromine species such as bromoform was present at the tropopause), also produces similar results. The loss rate of ozone due to bromine increases in proportion to the increase in Br_y (e.g., doubling at 14 km). The loss due to iodine, however, increases much less (e.g., 25% at 14 km) because the reaction of HO_2 with IO is calculated to account for most of the ozone loss by iodine below 15 km. Thus, the relative role of iodine compared to bromine would be even smaller if our photochemical model underestimates the concentration of BrO.

Catalytic removal of stratospheric ozone by iodine is very slow. For instance, even at the upper limit for our estimate of the iodine mixing ratio, 0.5 pptv, the lifetime of ozone with respect to chemical removal by iodine is more than 50 years at altitudes above 15 km (where the bulk of the stratospheric ozone column resides). This removal rate is extremely slow compared to the typical transport lifetime of stratospheric air (~2 years). Consequently, iodine chemistry can only be responsible for an insignificant fraction of the loss in the column of midlatitude ozone observed during the past several decades [*WMO/UNEP*, 1995].

Appendix

In the atmospheric spectra, obvious spectral features due to both water and NO_2 are present. Our analysis for IO is restricted to spectral regions not containing H_2O lines. However, the numerous absorption features of NO_2 preclude use of such a simple technique for removing its influence. In this appendix we detail how the NO_2 signature was removed from the atmospheric spectra and the potential error associated with this method. First, however, we show how use of high-resolution spectroscopy combined with a high-pass filter helps discriminate against broad spectral absorption features.

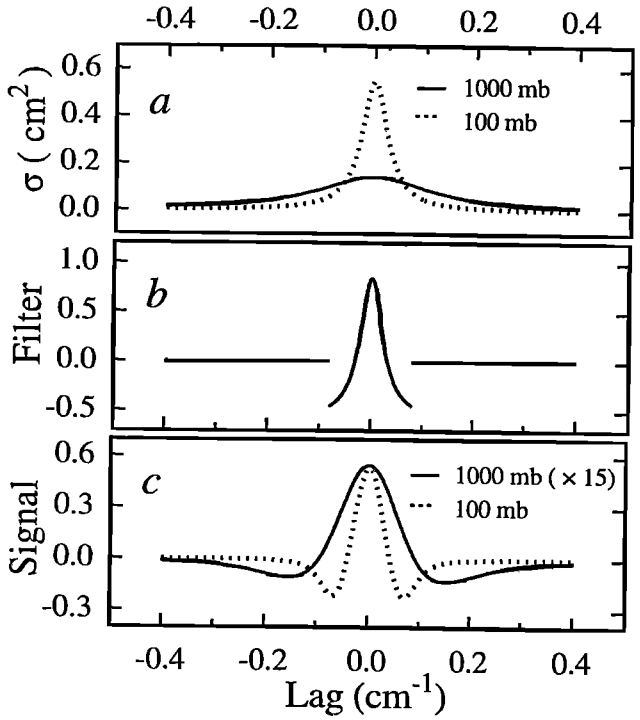

Figure A1. Pressure broadening and the IO gap function. (a) Absorption cross sections for a low-pressure stratospheric absorber (dashed) and a high-pressure boundary layer absorber (solid). The integrated cross sections are identical, but because of pressure broadening the peak cross section of the high-pressure absorber is significantly lower. (b) Gap filter designed for the low-pressure absorber. (c) Cross correlation of the gap filter with the high- and low-pressure absorber. The sensitivity to the high-pressure absorber is smaller by a factor of 15.

Pressure Broadening and Solar Spectroscopy

The spectral lineshapes of both IO and NO_2 exhibit very strong pressure dependent broadening. This feature is useful to this study because it provides a means of minimizing the influence of tropospheric absorbers. We illustrate the basic principle in Figure A1. In Figure A1a, two lineshapes are shown. The dashed line is a near-Lorentzian absorption lineshape of 0.07 cm^{-1} full width at half maximum (FWHM), similar to the lineshape of the lifetime- and pressure-broadened stratospheric IO rotational features. The solid line shows a Lorentzian absorption lineshape of 0.27 cm^{-1} FWHM, similar to lineshape of IO at 1 atm total pressure. The peak cross section for the pressure-broadened lineshape is a factor of 4 lower than the low-pressure cross section. Thus, our sensitivity to an absorber present in the boundary layer is considerably smaller than one present in the stratosphere. Our sensitivity to this pressure-broadened absorber is further reduced by the use of the cross-correlation technique. The gap filter used in this study (Plate 1c) is optimized for narrow absorbers and it acts as a high-pass filter. This is illustrated in Figure A1 also. In Figure A1b a gap filter designed for the low-pressure lineshape is shown. In Figure A1c

the cross correlation of this filter with both the high-pressure (solid) and low-pressure (dashed) spectra is plotted. For the same column of IO we are nearly 15 times less sensitive to boundary layer IO than stratospheric IO.

Application to NO_2

NO_2 is present in the atmosphere predominantly in the planetary boundary layer (Kitt Peak: $T = 280$ K; $p = 800$ mbar) and in the mid and upper stratosphere ($210 < T < 240$ K; $p < 50$ mbar). Many studies of atmospheric NO_2 have been performed by visible wavelength absorption spectroscopy [e.g., *Noxon et al.*, 1979]. All of these measurements have been performed with relatively low resolution spectrometers. It is well known that the NO_2 absorption cross sections are temperature dependent, and efforts have been made to account for this effect in these studies. In this work, because very high spectral resolution is employed, we have investigated the pressure dependence of the NO_2 absorption cross sections as well.

Shown in Figure A2 is a small portion of the NO_2 spectrum taken in the laboratory with the same spectrometer used to measure the IO pressure broadening. The resolution of the spectra is approximately 0.05 cm^{-1}. The solid thin and dashed lines are the spectra taken at temperatures of 240 and 298 K, respectively, at a pressure of less than 10 mbar. The thick solid line is the spectrum taken at 800 mbar 298 K. Dramatic changes due to pressure broadening of the NO_2 rotational lines are observed. Small but discernible changes are also seen in the two low-pressure spectra taken at different temperatures.

In Figure A3, the cross correlation of the IO gap filter used in this study with the NO_2 laboratory spectra is shown. The column density of NO_2 used to generate this figure corresponds to the typical column present in the spectra taken from Kitt Peak at high zenith angle ($\sim 2 \times 10^{16}$ molecule cm^{-2}). It is clear that any NO_2 present in the boundary layer is very inefficiently detected. The slant column in this figure would be equivalent to a 2-km-thick boundary layer with a 1-ppbv mixing ratio of NO_2, much larger than can be expected in the early morning above Kitt Peak. The same column of NO_2 present in the stratosphere produces a signal nearly 10 times larger. Fortunately, the temperature dependence of the stratospheric signal is very weak. The rotational structure changes only slightly with temperature at the spectral resolution employed here (0.05 cm^{-1}), and the cross correlation with the IO gap filter is quite insensitive to these small changes. This demonstrates that very high resolution absorption spectroscopy may be useful for measuring the stratospheric NO_2 column with minimal interference from boundary layer pollution.

To determine how NO_2 could influence our measurement of the IO column, we carried out the same analysis performed in section 6 without first accounting for absorption due to NO_2. Without removing the spectral features due to NO_2, the cross correlation of the IO gap with the atmospheric transmission spectra produces an estimate for the IO slant column change between SZA = 88° and 60° of $0 \pm 8 \times 10^{12}$ molecule cm^{-2}. The "noise" in the cross correlation increases by a factor of 2, and is highly correlated with the residuals shown in Fig. A3. Furthermore, because the cross correlation signal at zero lag is negative, the atmospheric NO_2 leads to an underestimate of the IO column.

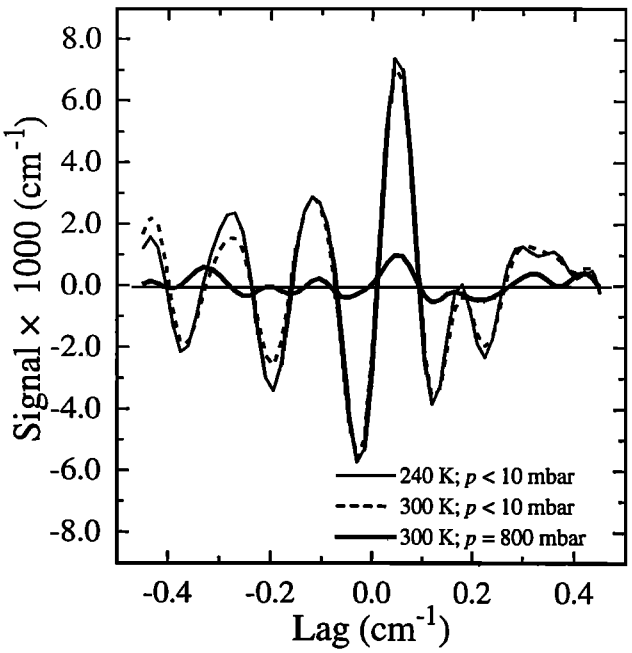

Figure A3. The cross correlation of the IO gap filter used in this study with a slant column of NO_2 typical of the high air mass atmospheric spectra (2.5×10^{16} molecule cm^{-2}). Shown in the thin solid and dashed lines are the signals produced from the low-pressure (<10 mbar) laboratory NO_2 spectra obtained at temperatures of 240 and 300 K, respectively. The temperature dependence is quite weak. Shown in the thick solid line is the signal produced from the same column of NO_2 at 800 mbar. Because of the pressure broadening, our observations are insensitive to the presence of NO_2 in the polluted boundary layer.

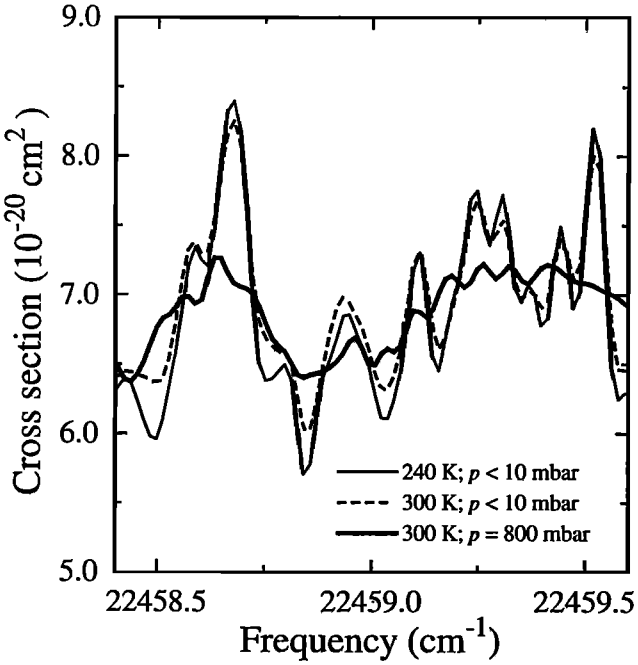

Figure A2. A small portion of the NO_2 spectrum near 22,460 cm^{-1}. Shown in the thin solid and dashed lines are the NO_2 cross sections taken at low pressure (< 10 mbar) and at temperatures of 240 and 300 K, respectively. At cold temperatures the spectral lines narrow and the differential cross sections increase slightly. Shown in the thick solid line is the cross section at 800 mbar and 300 K. Pressure broadening removes essentially all the high-resolution structure seen in the low-pressure spectrum.

For the analysis performed in this work, the low-temperature, low-pressure laboratory NO_2 spectrum (Fig. A2) is first fit to the atmospheric transmission in regions away from solar lines, telluric water lines, or any IO lines. The appropriate NO_2 signal is then subtracted from the entire spectrum. Because the full NO_2 column produces a negative IO signal nearly as large as the IO column determined in this study, care must be taken in matching the atmospheric residual to the laboratory spectrum. For example, to ensure that the retrieved IO signal is not affected significantly (± 25%) by absorption due to NO_2, the stratospheric NO_2 residuals must be matched to within 25%. Fortunately, because there are numerous strong NO_2 lines throughout the spectrum, this is accomplished quite easily (see Plate 2).

Acknowledgments. We would like to thank the many individuals and programs that contributed to this work At Harvard, support for the purchase of the Bruker FTS was provided through grants from the National Science Foundation (ATM-8921312) and the Empire State Electric Energy Research Corporation. Support for P.O.W. and T.F.H. was provided by the National Aeronautical and Space Administration (NASA) Upper Atmosphere Research Program (NAG-1-1305). At Kitt Peak we would like to thank the National Solar Observatory for use of the McMath-Pierce telescope and the solar spectrometer. Research by R.J.S. at the Jet Propulsion Laboratory, California Institute of Technology, was performed under contract with NASA. Paul Newman from NASA Goddard kindly provided information on the tropopause height above Kitt Peak. We thank M.J. Kurylo, A. R. Ravishankara, and J -P. Pommereau for sharing information from their laboratories on the kinetics and photochemistry of iodine prior to publication. Finally, we would also like to thank Kathy Perkins, Kelly Chance, Stan Sander, and Susan Solomon for their comments on the manuscript.

References

Arpag, K.H., P V. Johnston, H L. Miller, R.W Sanders, and S. Solomon, Observations of the stratospheric BrO column over Colorado, 40° N, *J. Geophys. Res*, 99, 8175-8181, 1994.

Atkinson, R., D L Baulch, R.A. Cox, R.F. Hampson Jr., J.A Kerr, and J. Troe, Evaluated kinetic and photochemical data for atmospheric chemistry, *J Phys. Chem Ref. Data, 21*, suppl. 4, 1125-1568, 1992.

Avallone, L M., D.W Toohey, S M Schauffler, W.H. Pollock, L.E. Heidt, E.L. Atlas, and K.R. Chan, In situ measurements of BrO during AASE II, *Geophys Res. Lett*, *22*, 831-834, 1995.

Barnes, I., K H Becker, and J Starcke, Fourier-Transform IR spectroscopic observations of gaseous nitrosyl iodine, nitryl iodine, and iodine nitrate, *J. Phys Chem., 95*, 9736-9740, 1991.

Bekooy, J.P., W.L. Meerts, and A. Dymanus, High-resolution laser-RF spectroscopy on the $A\ ^2\Pi_{3/2} \leftarrow X\ ^2\Pi_{3/2}$ system of iodine oxide (IO), *J. Mol. Spectrosc., 102*, 320-343, 1983.

Brault, J.W , Solar Fourier transform spectroscopy, in *Osservazioni e Memorie dell' Osservatorio Astrofisico di Arcetri, Proceedings of the JOSO Workshop*, edited by G. Godoli, G. Noci and A. Righini, pp. 33-50, Tip, Baccini, and Chiappi, Florence, 1978.

Brault, J W., Detection of electric quadrupole transitions in the oxygen *A* band at 7600Å, *J. Mol. Spectrosc., 80*, 384-387, 1980.

Brault, J.W , Fourier transform spectrometry, in *High Resolution in Astronomy, Proceedings of the 15th Advanced Course of the Swiss Society of Astronomy and Astrophysics, Saas-Fee*, edited by A.O. Benz, M.C.E. Huber, and M. Mayor, pp. 1-61, Observatoire de Genève, Souverny, 1985.

Brune, W.H., D.W. Toohey, J.G. Anderson, W.L. Starr, J.F. Vedder, and E.F. Danielsen, In situ northern mid-latitude observations of ClO, O_3, and BrO in the wintertime lower stratosphere, *Science, 242*, 558-562, 1988.

Camy-Peyret, C., J.M. Flaud, L. Delbouille, G. Roland, J.W. Brault, and L. Testerman, Quadrupole transitions of the 1-0 band of N_2 observed in a high resolution atmospheric spectrum, *J. Phys. Lett. 42*, L279-L283, 1981.

Chance, K., W.A. Traub, D.G. Johnson, K.W. Jucks, P. Ciarpallini, R.A. Stachnik, R.J. Salawitch, and H.A. Michelsen, Simultaneous measurements of stratospheric HO_x, NO_x, and Cl_x: Comparison with a photochemical model, *J. Geophys. Res., 101*, 9031-9043, 1996.

Cox, R.A. and G B. Coker, Absorption cross section and kinetics of IO in the photolysis of CH_3I in the presence of ozone, *J. Phys. Chem., 87*, 4478-4484, 1983.

Davis, D., J. Crawford, S. Liu, S. McKeen, A. Bandy, D. Thornton, F. Rowland, and D. Blake, Potential impact of iodine on tropospheric levels of ozone and other critical oxidants, *J. Geophys. Res., 101*, 2135-2147, 1996.

DeMore, W.B., S.P. Sander, C.J. Howard, A.R. Ravishankara, D.M. Golden, C.E. Kolb, R.F. Hampson, M.J. Kurylo, and M.J. Molina, Chemical kinetics and photochemical data for use in stratospheric modeling, Evaluation Number 11, *JPL Pub, 94-26*, Jet Propul. Lab., Pasadena, Calif., 1994.

Durie, R.A., F. Legay, and D.A. Ramsay, An emission system of the IO molecule, *Can. J. Phys., 38*, 444-452, 1960.

Fish, D.J., R.L. Jones, and E.K. Strong, Midlatitude observations of the diurnal variation of stratospheric BrO, *J. Geophys. Res. 100*, 18863-18871, 1995.

Gao, R.S., et al., Partitioning of the reactive nitrogen reservoir in the lower stratosphere of the southern hemisphere: Observations and modeling, *J. Geophys. Res.*, in press, 1997.

Gunson, M.R., C.B Farmer, R.H. Norton, R. Zander, C.P. Rinsland, J.H. Shaw, and B -C Gao. Measurements of CH_4, N_2O, CO, H_2O, and O_3 in the middle atmosphere by the Atmospheric Trace Molecule Spectroscopy experiment on Spacelab 3, *J. Geophys. Res., 95*, 13867-13882, 1990.

Hanson, D.R., A.R. Ravishankara, and E.R. Lovejoy, Reaction of $BrONO_2$ with H_2O on submicron sulfuric acid aerosol and the implications for the lower stratosphere, *J. Geophys Res., 101*, 9063-9069, 1996.

Herzberg, G., *Molecular Spectra and Molecular Structure*, vol 1, *Spectra of Diatomic Molecules*, Van Nostrand Reinhold, New York, 1950.

Himmelmann, S., J. Orphal, H. Bovensmann, A. Richter, A. Ladstätter-Weisenmayer, and J.P. Burrows, First observation of the OIO molecule by time-resolved flash photolysis absorption spectroscopy, *Chem. Phys Lett., 251*, 330-334, 1996.

Inoue, G., M. Suzuki, and N. Washida, Laser induced fluorescence of IO radicals and rate constant for the reaction of IO + NO, *J. Chem. Phys., 79*, 4730-4735, 1983.

Jenkin, M E., and R.A. Cox, Kinetics study of the reactions IO + NO_2 + M → $IONO_2$ + M, IO + IO → Products and I + O_3 → IO + O_2, *J. Phys. Chem., 89*, 192-199, 1985.

Keating, G.M., and D.F. Young, Interim reference ozone models for the middle atmosphere, in *Handbook for MAP*, vol. 16, edited by K. Labitzke, J.J. Barnett, and B. Edwards, pp. 205-229, SCOSTEP Secretariat, Univ of Ill., Urbana, 1985.

Keim, E.R., et al., Observations of large reductions in the NO/NO_y ratio near the mid-latitude tropopause and the role of heterogeneous chemistry, *Geophys. Res. Lett. 23*, 3223-3226, 1996.

Larson, H.P., R R. Treffers, and U. Fink, Phosphine in Jupiter's atmosphere. The evidence from high-altitude observations at 5 micrometers, *Astrophys. J., 211*, 972-979, 1977.

Laszlo, B., M.J. Kurylo, and R.E. Huie, Absorption cross sections, kinetics of formation, and self-reaction of the IO radical produced via the laser photolysis of N_2O/I_2 mixtures, *J. Phys. Chem., 99*, 11701-11707, 1995.

Laszlo, B., R.E Huie, M.J. Kurylo, and A.W. Miziolek, Kinetic studies of the reaction of BrO and IO radicals, *J. Geophys. Res.*, in press, 1997.

McCormick, M.P., J.M. Zawodny, R.E. Veiga, J.C. Larsen, and P.H. Wang, An overview of SAGE I and II ozone measurements, *Planet. Space Sci., 37*, 1567-1586, 1989.

Murcray, D.G., T.G. Kyle, F.H. Murcray, and W.J. Williams, Nitric acid and nitric oxide in the lower stratosphere, *Nature, 218*, 78-79, 1968.

Noxon, J.F., E.C. Whipple Jr., and R.S. Hyde, Stratospheric NO_2. 1. Observational method and behavior at mid-latitude, *J. Geophys. Res., 84*, 5047-5065, 1979.

Pierce, A.K., and J.B. Breckinridge, The Kitt Peak table of photographic solar spectrum wavelengths, *Contrib. 559*, Kitt Peak Nat. Obs., Kitt Peak, Ariz, 1974.

Pundt, I., J.-P. Pommereau, C. Phillips, and E. Lateltin, Upper limit of iodine oxide in the lower stratosphere, *J. Atmos. Chem.*, in press, 1997.

Rao, M.L.P., D.V.K. Rao, and P.T. Rao, Dissociation energies, r-centroids and Franck-Condon factors of IO molecule, *Phys. Lett., 50A*, 341-342, 1974.

Rinsland, C.P., A. Goldman, and G.M. Stokes, Identification of atmospheric C_2H_2 lines in the 3230-3340 cm^{-1} region of high resolution solar absorption spectra recorded at the National Solar Observatory, *Appl. Opt., 24*, 2044-2046, 1985.

Rothman, L.S., Update of the AFGL atmospheric absorption line parameters compilation, *Appl. Opt., 17*, 3517-3518, 1978.

Salawitch, R.J., S.C. Wofsy, and M.B. McElroy, Chemistry of OClO in the

Antarctic stratosphere: Implications for bromine, *Planet. Space Sci., 36,* 213-224, 1988.

Salawitch, R.J., et al., The diurnal variation of hydrogen, nitrogen, and chlorine radicals: Implications for the heterogeneous production of HNO_2, *Geophys. Res. Lett., 21,* 2551-2554, 1994a.

Salawitch, R.J., et al., The distribution of hydrogen, nitrogen, and chlorine radicals in the lower stratosphere: Implications for changes in O_3 due to emission of NO_y from supersonic aircraft, *Geophys. Res. Lett., 21,* 2547-2550, 1994b.

Sander, S.P., Kinetics and mechanism of the IO + IO reaction, *J. Phys. Chem., 90,* 2194-2199, 1986.

Schauffler, S.M., L.E. Heidt, W.H. Pollock, T.M. Gilpin, J.F. Vedder, S. Solomon, R.A. Lueb, and E.L. Atlas, Measurements of halogenated organic compounds near the tropical tropopause, *Geophys. Res. Lett., 20,* 2567-2570, 1993.

Solomon, S., J.B. Burkholder, A.R. Ravishankara, and R.R. Garcia, Ozone depletion and global warming potentials of CF_3I, *J. Geophys. Res., 99,* 20929-20935, 1994a.

Solomon, S., R.R. Garcia, and A.R. Ravishankara, On the role of iodine in ozone depletion, *J. Geophys. Res., 99,* 20491-20499, 1994b.

Stickel, R.E., A.J. Hynes, J.D. Bradshaw, W.L. Chameides, and D.D. Davis, Absorption cross sections and kinetic considerations of the IO radical as determined by laser flash photolysis/laser absorption spectroscopy, *J. Phys. Chem., 92,* 1862-1864, 1988.

Turnipseed, A.A., M.K. Gillis, J.B. Burkholder, and A.R. Ravishankara, LIF detection of IO and the rate coefficients for I + O_3 and IO + NO reactions, *Chem. Phys. Lett., 242,* 427-434, 1995a.

Turnipseed, A.A., M.K. Gillis, J.B. Burkholder, and A.R. Ravishankara, Iodine chemistry in the stratosphere: Kinetics of the IO + ClO and IO + BrO reactions (abstract), *EOS Trans. AGU, 76* (45), Fall Meet. Suppl., F116, 1995b.

Vaidya, W.M., The flame spectra of some aliphatic halides: Part 1, *Proc. Indian Acad. Sci. Sect. A., 6,* 122-128, 1938.

Woodbridge, E.L., et al., Estimates of total organic and inorganic chlorine in the lower stratosphere from in situ and flask measurements during AASE II, *J. Geophys. Res., 100,* 3057-3064, 1995.

World Meteorological Organization/United Nations Environment Programme (WMO/UNEP), Scientific Assessment of Ozone Depletion: 1994, *WMO Rep. 37,* Geneva, 1995.

J. W. Brault, Department of Chemistry and Biochemistry, University of Colorado, Boulder, CO 80309 (e-mail: brault@noao.edu)

T. F. Hanisco and P.O. Wennberg, Department of Chemistry and Chemical Biology, Harvard University, 12 Oxford St., Cambridge, MA 02138. (e-mail: tfh@huarp.harvard.edu, wennberg@huarp.harvard.edu)

G. H. Mount, NOAA Aeronomy Laboratory, 325 Broadway, Boulder, CO 80307 (e-mail: mount@al.noaa.gov)

R. J. Salawitch, Jet Propulsion Laboratory, Pasadena, CA 91109. (e-mail: rjs@caesar.jpl.nasa.gov)

(Received January 3, 1996; revised November 17, 1996;
accepted November 18, 1996.)